Weather and Climate Extremes 33 (2021) 100345

Contents lists available at ScienceDirect

Weather and Climate Extremes

journal homepage: www.elsevier.com/locate/wace

Beyond El Niño: Unsung climate modes drive African floods

Andrea Ficchì [a,*], Hannah Cloke [a,b,c,d], Claudia Neves [e], Steve Woolnough [b,f], Erin Coughlan de Perez [g], Ervin Zsoter [a,h], Izidine Pinto [i], Arlindo Meque [j], Elisabeth Stephens [a]

[a] Department of Geography and Environmental Science, University of Reading, Reading, UK
[b] Department of Meteorology, University of Reading, Whiteknights, UK
[c] Department of Earth Sciences, Uppsala University, Uppsala, Sweden
[d] Centre of Natural Hazards and Disaster Science, CNDS, Uppsala, Sweden
[e] Department of Mathematics and Statistics, University of Reading, Reading, UK
[f] National Centre for Atmospheric Science, University of Reading, Reading, UK
[g] Red Cross Red Crescent Climate Centre, The Hague, 5 2521, CV, the Netherlands
[h] European Centre for Medium-Range Weather Forecasts, Shinfield Park, Reading, UK
[i] Climate System Analysis Group (CSAG), University of Cape Town, Cape Town, South Africa
[j] Southern African Development Community (SADC) Climate Services Centre, Gaborone, Botswana

ARTICLE INFO

Keywords:
Climate variability
Flood frequency analysis
Teleconnections
El Niño–Southern Oscillation
Indian Ocean Dipole
Tropical South Atlantic

ABSTRACT

The El Niño Southern Oscillation (ENSO) dominates the conversation about predictability of climate extremes and early warning and preparedness for floods and droughts, but in Africa other modes of climate variability are also known to influence rainfall anomalies. In this study, we compare the role of ENSO in driving flood hazard over sub-Saharan Africa with modes of climate variability in the Indian and Atlantic Oceans. This is achieved by applying flood frequency approaches to a hydrological reanalysis dataset and streamflow observations for different phases of the ENSO, Indian Ocean Dipole and Tropical South Atlantic climate modes.

Our results highlight that Indian and Atlantic Ocean modes of climate variability are equally as important as ENSO for driving changes in the frequency of impactful floods across Africa. We propose that in many parts of Africa a larger consideration of these unsung climate modes could provide improved seasonal predictions of associated flood hazard and better inform adaptation to the changing climate.

1. Introduction

Precipitation variability in Africa is influenced by complex interactions between various weather and climate patterns acting at local and global scales. At the global scales, the El Niño–Southern Oscillation (ENSO) was identified as one of the primary drivers of precipitation Nicholson, 2017; (Nicholson and Kim, 1997). By exploiting the influence of ENSO on precipitation (e.g. Cai et al., 2011; Rowell, 2013; Trenberth and Caron, 2000) and river flows (Emerton et al., 2017; Su et al., 2018; Ward et al., 2014b) skilful forecasts of an upcoming El Niño/La Niña event are frequently used by scientists to provide early warning of floods and droughts at seasonal timescales allowing for early action by governments and non-governmental organizations (Coughlan de Perez et al., 2015; Guimarães Nobre et al., 2019; Tozier de la Poterie et al., 2018). ENSO dominates the conversations around international coordination of preparedness activities, with UN agencies resolving to take action at a 55% probability threshold of an ENSO event developing (IASC, 2018). On the part of climate scientists, how ENSO might change with global warming is considered "one of the most important issues in climate change science" (Cai et al., 2015). However, besides ENSO, there are other modes of climate variability in the Indian and Atlantic Oceans emerging as important and predictable independent drivers of rainfall variability in Africa (e.g. Camberlin et al., 2001; Florenchie et al., 2003; Preethi et al., 2015; Shi et al., 2012).

For example, the Indian Ocean Dipole (IOD) (Saji et al., 1999) affects seasonal rainfall anomalies and extreme hydrological conditions mainly across eastern and southern-Africa (Behera et al., 2005; Black, 2005; Manatsa et al., 2008; Marchant et al., 2007; Washington and Preston, 2006; Wenhaji Ndomeni et al., 2018). Sea Surface Temperatures (SST) patterns in the Tropical South-east Atlantic have also been linked with regional rainfall anomalies mainly across western, southern and Sahelian Africa (Camberlin et al., 2001; Polo et al., 2008; Rouault et al.,

* Corresponding author.
E-mail address: a.ficchi@reading.ac.uk (A. Ficchì).

https://doi.org/10.1016/j.wace.2021.100345
Received 2 November 2020; Received in revised form 25 June 2021; Accepted 29 June 2021
Available online 30 June 2021

2003; Rowell, 2013).

Whereas the impact of ENSO on river flows has been well studied at global and continental scales (e.g. Emerton et al., 2017; Su et al., 2018; Ward et al., 2014b), a comparison with the impact of other modes of climate variability would provide a better understanding of what drives flood hazard across the African continent, informing both improved preparedness for floods and a better understanding of how flood hazard will be affected by the changing climate.

This study aims to investigate the effects of ENSO, IOD and Tropical South-Atlantic (TSA) SST modes on flood hazard over Africa through answering the following research questions:

- What are our main findings on the effects of ENSO on flood hazard and how do they compare with the literature? In order to be able to compare the importance of ENSO with other modes, we want to ensure that our results with ENSO are consistent with the previous literature.
- What is the relative weight of different climate modes on floods at the continental scale? Is there a dominant mode among these Indian, Pacific and Atlantic Ocean modes?
- Where is each climate mode dominant? Are there any strong spatial signals?
- Can these climate modes be used for flood forecasting?
- What are the implications of our results for the assessment of flood hazard under climate change?

Previous studies have shown the importance of focusing directly on the streamflow rather than rainfall to characterise flood hazard and teleconnections (Emerton et al., 2017; Ficchì and Stephens, 2019) because of the non-linearities between precipitation and flood characteristics along with integration of rainfall variabilities spatially and temporally. Here we use the 0.1°-resolution 36-year global-scale streamflow reanalysis (ECMWF, 2018) from the Copernicus-Emergency Management Service (CEMS-GloFAS) model (Alfieri et al., 2013) which is the latest verified hydrological reanalysis over Africa incorporating rainfall bias corrections (Balsamo et al., 2015; Ficchì and Stephens, 2019), described in Section 2, Data and Methods. We focus on a 5-year return period streamflow magnitude as representative of a moderately extreme albeit impactful flood and we analyse the changes in its likelihood during past ENSO, IOD and TSA events. The choice of a 5-year return period flood is in line with the minimum size of a flood event that is usually targeted by humanitarian funding mechanisms for Forecast-based Financing (Coughlan de Perez et al., 2015), such as the International Federation of Red Cross and Red Crescent Societies' (IFRC) Disaster Relief Emergency Fund (DREF).

Fig. 1 shows the river network modelled in sub-Saharan Africa (SSA), where composite flood probabilities have been calculated for the different climate modes based on simulated annual floods, extreme value analysis techniques and observed SST indices (see Section 2, Data and Methods). The reanalysis allows the provision of a spatially continuous and temporally-consistent picture of climate variability impacts on floods over the continent, while stream-gauge observations are available only for a minor part of flood-prone regions of Africa over a sufficiently long period. We also use an observational dataset from the Global Runoff Data Centre (BfG, 2017) at 48 stream-gauges with longer time series (Fig. 1) to compare the climate variability impacts detected in the reanalysis with observations covering some major African river basins, including the Congo, Nile, Niger and Zambezi.

2. Data and methods

2.1. Streamflow reanalysis dataset

We use a daily 0.1°-resolution streamflow reanalysis covering 1980–2015 (ECMWF, 2018) produced by a global-scale hydrological model, the Copernicus-Emergency Management Service's Global Flood

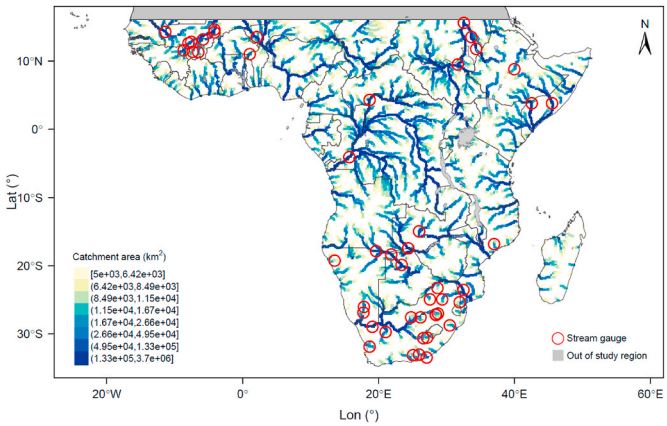

Fig. 1. Map of sub-Saharan Africa with the river network cells of the streamflow reanalysis (GloFAS) with upstream catchment area larger than 5000 km^2 (18118 grid points at 0.1° resolution) showing the distribution of catchment areas (km^2) and the location of 48 stream gauges selected based on data available over 1980–2015 (red dots). (For interpretation of the references to colour in this figure legend, the reader is referred to the Web version of this article.)

Awareness System, GloFAS (Alfieri et al., 2013). To derive this reanalysis, the LISFLOOD global-scale hydrological routing model used in GloFAS (Van Der Knijff et al., 2010) is forced with the ERA-Interim/Land meteorological reanalysis, incorporating the Global Precipitation Climatology Project (GPCP) - based bias corrections, coupled with the H-TESSEL land-surface model (Balsamo et al., 2015). The hydrological reanalysis produced with ERA-Interim/Land showed a good correlation with observations across Africa in terms of monthly runoff volumes from H-TESSEL (Balsamo et al., 2015) and annual flood timing from GloFAS (Ficchì and Stephens, 2019), indicating that this dataset is a suitable proxy to observations to analyse climate variability impacts. By using a reanalysis dataset that is not calibrated with stream gauge data (GloFAS version 1.0) and not including most human influences (abstractions and reservoirs) on river flows, we exclusively focus on the impacts of climate variability on streamflow, avoiding the impacts of human influence on some stream gauge data. Whereas suitable stream gauge data across the African continent are limited (especially in publicly available archives), reanalysis data also provides significant advantages including a temporally-consistent data period and spatially-continuous coverage over the continent.

We extract the annual maximum (AMAX) flow for 18118 river gridcells in sub-Saharan Africa (SSA, study area: −17.75 to 51.25 longitude, −34.75 to 16.05 latitude) with an upstream area >5000 km^2 (see Fig. 1). There is an even degree of coverage of mesoscale (upper and lower) to large-scale or macroscale river basin sizes across SSA. To ensure annual flood maxima are only considered which lag climate variability events, we set a hydrological year start date of May 1st, and we analyse the effects of each climate mode phase on the hydrological year starting in May of the calendar year in which the SST anomalies start to develop and peak (see Table 1 and discussion on the seasonality of the climate modes considered in Section 2.3). The independence of subsequent annual maxima is verified by keeping a selected annual maximum flood peak only if separated by at least two months from the previous annual maximum flow.

2.2. Streamflow observations

We use daily streamflow observations from the Global Runoff Data Centre (GRDC) to evaluate our results using the reanalysis against an observed reference for tens of river basins where long records are available. Long data records (>30 years) with low gaps (<5% per year) were available only for around 50 stations across Africa, mostly falling

Table 1
Hydrological years categorised as positive and negative phases of ENSO, IOD and TSA over the 36-year period 1980–2015 based on the tercile approach described in Section 2, Data and Methods. The years in each category correspond to the calendar years when the SST anomalies start to develop and peak.

Climate mode	Hydrological year
ENSO +	1982, 1986, 1987, 1991, 1994, 1997, 2002, 2004, 2006, 2009, 2014, 2015
ENSO –	1983, 1984, 1988, 1995, 1998, 1999, 2000, 2005, 2007, 2008, 2010, 2011
IOD +	1982, 1983, 1987, 1991, 1994, 1997, 2002, 2006, 2007, 2011, 2012, 2015
IOD –	1980, 1981, 1984, 1985, 1986, 1989, 1990, 1992, 1996, 1998, 2010, 2013
TSA +	1984, 1988, 1995, 1996, 1998, 1999, 2003, 2008, 2009, 2010, 2011
TSA –	1980, 1981, 1982, 1983, 1990, 1991, 1992, 1994, 1997, 2004, 2012

within the top six major African river basins (Congo, Nile, Niger, Zambezi, Orange and Jubba-Shabelle). To evaluate the results obtained using the reanalysis, we applied the same method for annual maxima detection and flood frequency analysis to the streamflow observations dataset, over the same period as the reanalysis. Strict criteria on data availability were necessary to select stream gauge observations with sufficient sample size to apply a flood frequency analysis framework as done for the reanalysis: forty-eight stream gauges were selected (Fig. 1) over the 36-year study period of the reanalysis with (i) $>$ 27 years of observations available within the study period, with gaps rate lower than 5% per year, (ii) at least six hydrological years per phase of ENSO/IOD/TSA (see Table 1), and (iii) no gap-filling artifacts or evidence of water management influencing the flood peaks. Analogously, some stream gauges were selected over the longer period 1950–2016, with at least 40 years of daily data with gaps rate less than 5% per year. This longer period was used to assess the effects of co-occurring modes over a larger sample of annual maxima, matching the period of SST records for ENSO/IOD/TSA indices available before the reanalysis start (see Supplementary Tables S1 and S2).

2.3. Climate variability modes: choice and definition

The climate variability modes considered in this study are ENSO, the Indian Ocean Dipole (IOD) and the Tropical South Atlantic (TSA) SST mode. We chose these based on the following three factors: (i) literature evidence of the effects of these modes on large-scale seasonal rainfall variability across Africa, (ii) similar frequency of the warm and cold events of each mode (about every 3–5 years; see Supplementary Fig. S1) so that the same methodological approach can be applied, and (iii) significant independence between the modes considered, despite a high rate of cooccurrence of two pairs of positive/negative phases (i.e. ENSO+/IOD+ and ENSO-/TSA+; see Supplementary Fig. S2 and Table S1).

ENSO has been traditionally pointed to as the primary climate mode driving rainfall variability across Africa (Nicholson, 2017; Nicholson and Kim, 1997). In terms of floods, ENSO positive phase (El Niño) events are well established as leading to wet (positive) rainfall anomalies in equatorial eastern Africa short rains during the OND season (Nicholson, 2017; Nicholson and Kim, 1997). ENSO negative phase (La Niña) events have been linked with wetter than normal conditions and floods in southern Africa, especially in the austral summer rainfall regions such as eastern/northern South Africa and Mozambique (Jury and Lucio, 2004; Reason and Rouault, 2002). However, there are significant differences from one ENSO episode to another which have been linked to simultaneous independent anomalies in western Indian and eastern tropical South Atlantic Oceans (Lyon and Mason, 2007; Preethi et al., 2015). In this study we use the Oceanic Niño Index (ONI), i.e. 3-month running means of SST anomalies in the Niño 3.4 region (Trenberth, 1997) to define positive and negative ENSO events.

The IOD is thought to be the most prominent pattern of SST variability in the Indian Ocean and is at least partially independent of ENSO (Saji et al., 1999), though there is a correlation between the positive phases (Wolff et al., 2011). The IOD has been linked with rainfall anomalies over Africa regardless of the ENSO state (Behera et al., 2005; Preethi et al., 2015; Saji and Yamagata, 2003). In terms of floods, during positive dipole mode events (IOD+), wet anomalies occur in eastern Africa short rains (Behera et al., 2005; Black, 2005), while negative phases (IOD-) lead to wet anomalies in southern regions (Behera et al., 2005; Saji and Yamagata, 2003). In this study we use the well-established Dipole Mode Index (DMI), i.e. the difference in SST anomaly between the tropical western Indian Ocean and the tropical south-eastern Indian Ocean (Saji et al., 1999), to define positive and negative IOD events.

In the Tropical Atlantic, several modes of variability are thought to exist, though there is no predominant standard index and SST region acknowledged in the literature (Lutz et al., 2013). Often, different SST patterns are considered in the South-eastern Atlantic basin facing the African coastline, such as the Benguela Niño off the Angolan coast and the Atlantic Niño in the equatorial Atlantic (Lutz et al., 2013). Moisture fluxes from the Benguela Niño region, driven by warm SST anomalies, have been linked to wet rainfall anomalies in south-western Africa, especially along the Angolan/Namibian coast (Rouault et al., 2003), but sometimes also to events further inland into south-eastern Africa, e.g. flooding in 2013 in Mozambique (Manhique et al., 2015). Cold South Atlantic SSTs are related to wet anomalies in the coastal West African monsoon region (northern hemisphere West SSA) and in the Gulf of Guinea area (Lutz et al., 2015; Reason and Rouault, 2006). In this study we use the Tropical South Atlantic (TSA) SST region (Enfield et al., 1999), which is a large-scale consistent index explaining most of the variance in tropical Atlantic SSTs, that has been found to explain interannual rainfall variability across several regions in Africa (Camberlin et al., 2001).

The phase of each climate mode is defined based on a tercile approach which categorizes negative (bottom 33%) and positive (upper 33%) values of the index associated with each mode of climate variability, giving a subset of a dozen years in each phase from the same 36-year period as the streamflow reanalysis (i.e. 12 years for all ENSO and IOD phases and 11 years for TSA positive/negative phases, as one year is removed for TSA phases due to an SST oscillation between positive and negative values; see Table 1). The 36-year period is deemed sufficiently long to obtain meaningful and robust values for the tercile-based thresholds for each SST index; this is evident, for example, for ENSO, for which the tercile thresholds for ONI come out to approximately $+0.5$ °C for El Niño and -0.5 °C for La Niña (see Supplementary Figs. S2a–b), very close to the well-known fixed thresholds defined by the NOAA's Climate Prediction Center (CPC).

The SST indices are taken from published timeseries derived using monthly global analysis products from the National Oceanic and Atmospheric Administration, NOAA (for ONI and TSA: https://www.esrl.noaa.gov/psd/data/; for DMI: www.esrl.noaa.gov/psd/gcos_wgsp/Timeseries/DMI/). Events were defined based on the maximum/minimum monthly values of the SST indices during the months when the SST peaks occur in each mode; for ENSO and IOD in boreal autumn/winter (August to December for ENSO and June to November for IOD), for TSA in boreal spring/summer (March to August, see Supplementary Fig. S3, showing the seasonality of the climate modes considered).

The co-occurrence rates of the climate modes considered in the study (Supplementary Table S1) show that two pairs of ENSO/IOD/TSA phases mostly co-occur over the 36-year period (ENSO+/IOD+ and ENSO-/TSA+, with co-occurrence $>$ 50%) and these pairs are the same over a longer 67-year period, with similar rates of co-occurrence. There is still significant independence between all modes considered, with low correlation between SST anomalies also for the most frequently co-occurring modes (Spierman's correlation, $\rho < 0.5$), confirming the value of looking at each mode independently over the 36-year period of

analysis. However, the small sample of years for composite analysis leads to some important limitations, in that we cannot disentangle the combined influence and interferences between different climate modes (co-occurring or not) and the impact of their diversity (e.g. intensity, timing and location of SST anomalies) on floods.

2.4. Flood-frequency analysis framework

At each location (river gridcell), we fitted a Generalized Extreme Value (GEV) distribution to the available sample of annual maxima and subsequently estimated the relevant shape and scale parameters via maximum likelihood. Confidence intervals (at a 95%-confidence level) were obtained through parametric bootstrapping (300 bootstrap iterations) using the 'extRemes' package in R (Gilleland and Katz, 2016). The whole AMAX dataset (36 values) was used to obtain the flood frequency curves for the climatology. From these curves the 5-year return period flow magnitude ($Q_{5\text{-}y}$) has been extracted as representative of an 'impactful flood', i.e. a flood severe enough to lead to societal impacts. Although focusing on larger return periods would be of interest, a 5-year return period was deemed a reasonable flood event size to obtain results with sufficient statistical confidence given the small sample size of hydrological years available (especially for the 12-year composites).

River gridcells presenting very dry conditions over the whole period were discarded, by removing gridcells with a 5-year return period flow lower than 10 m^3/s (3% of the model domain). River cells with unsatisfactory GEV fit were also discarded, if the ratio of fitted/'observed' quantiles is different from 1 by more than 25% and if the changes from climatology do not agree in sign between fitted vs. 'observed' quantiles.

The same approach is then applied to the composite samples of AMAX associated with each phase of the three climate modes considered (12 years for ENSO +/−, IOD +/− and 11 years for TSA +/−; see Table 1) and the return periods of the defined impactful flood magnitude ($Q_{5\text{-}y}$) are determined for each phase from the correspondent fitted quantile. As such, the estimated return periods represent the probability of the impactful flood occurring during (or within the year of development of) each climate mode event (ENSO +/−, IOD +/− and TSA +/−). Note that the climatology probability of a 5-year return period flow is 20%, so if the estimated probability is around 20% (e.g. ±5%) for a particular climate mode, the impactful flood is expected with a similar frequency as usual (climatology); accordingly, a probability of 40% represents a doubling of the likelihood of an impactful flood. In addition to the significance test (at 95%-confidence level) from the parametric bootstrapping, we have estimated additional confidence boundaries for significant changes in the probability (p_f) of a 5-year return period flow, by extracting the 10th/90th percentiles of the probability p_f obtained from randomised samples of 12 years from the whole 36-year period (non-parametric bootstrap). For a high number of bootstrap iterations (>100), these confidence boundaries of the climatology probability converge to 8.33% and 33.33% (10th and 90th percentiles respectively) over the whole domain. Thus, such values were used in maps for the classification of places where, in presence of the positive and negative phases of the three climate modes, the change in flood probability is particularly large with respect to possible random variations of the climatology probability over time. As additional statistical reference, the percentage of the SSA river network with significant changes (either increase or decrease) of impactful flood likelihood from these randomised samples was found to be 15%, representing a threshold to detect if changes are particularly widespread with respect to possible random variations of the climatology probability.

Thus, we are able to map the changes in the probability of an impactful flood (p_f) with respect to the 36-year climatology for different climate modes over the continent. By using the 95%-confidence intervals estimated via parametric bootstrapping, we are also able to assess whether the changes in flood hazard are significant. We can then compare these significant changes with those from randomised samples by looking at the confidence boundaries for the climatology probability and the percentage of river network significantly affected. Note that the uncertainty in the fitted GEV parameters can be quite high for such relatively short composite records, so the 95% confidence intervals are expected to be generally large and the significance test quite restrictive.

2.5. Evaluation of flood likelihood with climate indices in forecast mode

The flood probabilities estimated for different climate patterns can be used as predictions, once a seasonal SST mode is forecasted (by means of statistical or dynamical models) after propagating the probabilities of the SST forecast and of the flooding likelihood conditional on that mode. We compute reliability diagrams for these flood probabilities by following a leave-one-out cross-validation approach; the flood frequency distribution is fitted with one year removed from each composite sample, which is then used for validation by calculating the observed frequency of the impactful flood across all the gridcells following the methodology proposed by Horritt (2006). For each forecast probability bin (e.g. 10% range) an observed frequency is calculated. Then the cross-validation test is repeated for all possible validation years of the subsamples (12 years for ENSO/IOD and 11 years for TSA phases) for each climate mode considered and the mean of the observed frequency calculated.

3. Results

3.1. Effects of climate variability on flood hazard

There is a large spatial variability in the expected probability of the impactful flood for all climate modes (Fig. 2). Despite a high degree of uncertainty in the signal of flood likelihood change indicated by the bootstrap significance test, there are still multiple rivers across SSA with a significant difference in flood hazard with respect to all years (see Fig. 2 and Table 2). The main locations where flood likelihood increases or decreases significantly (p_f>25% or p_f<15% at a 95%-confidence level) can be summarized as:

(i) For ENSO + (Fig. 2a): flood likelihood increases in some river sections in southern parts of the Horn of Africa (mainly in Uganda, Kenya and South Somalia) and in a few river sections in central equatorial and western SSA (in the Democratic Republic of the Congo, DRC, and in Nigeria); it decreases in some river basins in southern Africa (below 20° S), the Lake Chad Basin (especially in Chad and Central African Republic), Nile basin in Sudan and the Ethiopian highlands as well as the Jubba-Shabelle rivers and several river sections across the Congo basin (especially in the DRC).

(ii) For ENSO – (Fig. 2b): flood likelihood increases in southern Africa (below 10° S) including long river sections of the Zambezi and Okavango Basins (in Angola, Botswana and Zambia) and the Rovuma and Lugenda Rivers (in northern Mozambique), in the Nile basin, and upstream river sections of the Congo basin; it decreases in some river sections in eastern Africa (including the Dawa River in Ethiopia, Kenya and Somalia, the Baro and Akobo rivers in Ethiopia and on the borders between South Sudan and Ethiopia) and in western SSA, in long river sections of the Niger Basin.

(iii) For IOD + (Fig. 2c): flood likelihood increases in southern parts of the Horn of Africa, especially in the Jubba River in southern Somalia, and in some river sections in central Africa, especially in long river sections in the Congo River basin (both downstream and upstream); it decreases in some rivers in southern Africa (and central-southern SSA, below 5° S), including sections of the Orange, Zambezi and upstream Congo basins, and in tropical northern SSA including the Nile basin although to a lesser extent than for ENSO+.

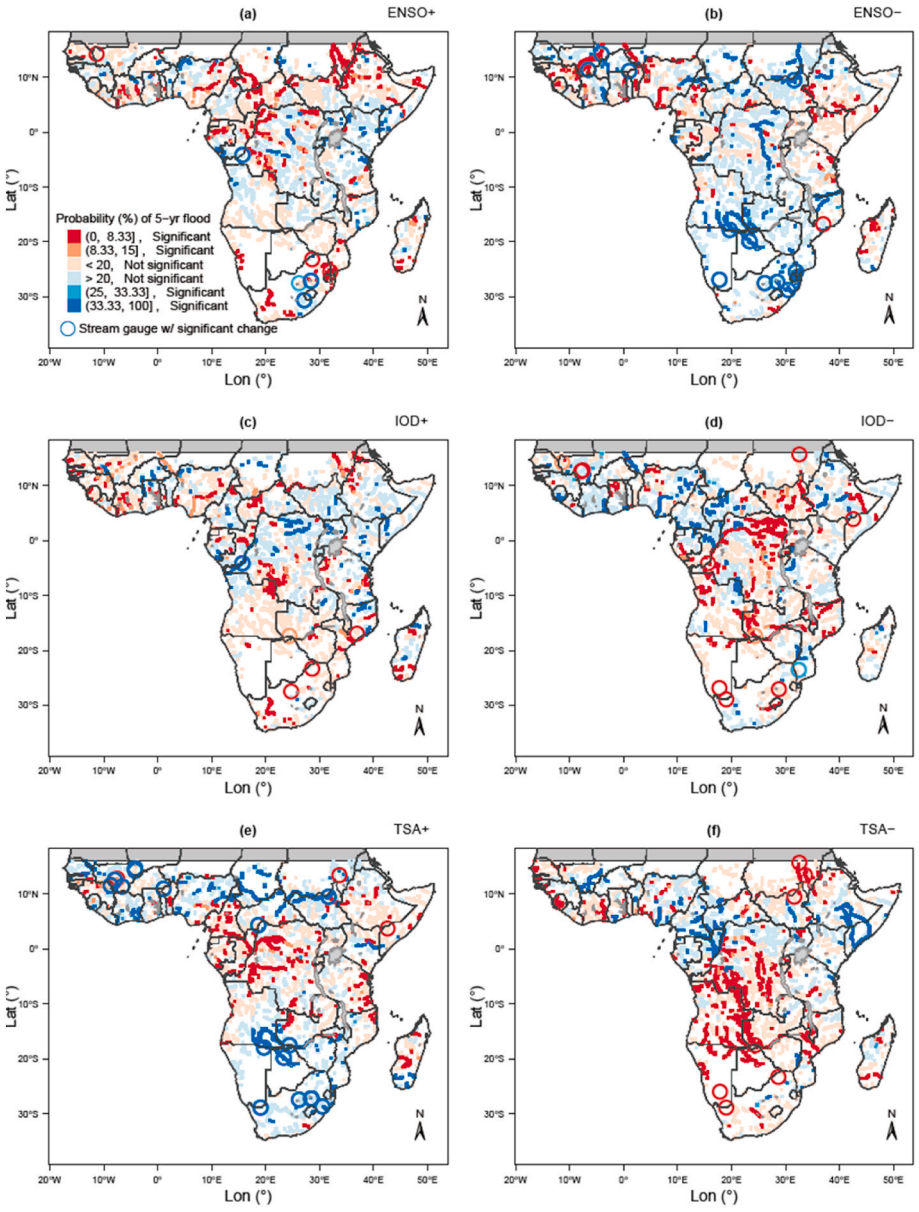

Fig. 2. Maps of changes of 5-year return level flood probabilities for positive and negative ENSO, IOD, TSA phases with respect to the climatology (1980–2015): (a) ENSO +, (b) ENSO –, (c) IOD +, (d) IOD –, (e) TSA +, and (f) TSA – years. Strongest red/blue colours are for significant changes (decrease/increase) in probability with 95% confidence level (with respect to climatology probability of 20%); the lowest/highest bounds (8.33%/33.33%) correspond to additional confidence boundaries for the climatology probability from randomised samples of years (non-parametric bootstrap). The coloured river cells represent the result from the reanalysis, while stream gauges with significant changes are shown with empty circle dots. River cells with unsatisfactory GEV fit are blanked (see Section 2, Data and Methods). (For interpretation of the references to colour in this figure legend, the reader is referred to the Web version of this article.)

Table 2
Summary statistics of percentage of sub-Saharan Africa (SSA) river network affected by significant changes in impactful (5-year return period) flood likelihood during ENSO, IOD and TSA positive and negative phases. River cells with unsatisfactory GEV fit are not considered as in Fig. 2 (see Section 2, Data and Methods). The statistics for flood likelihood increase are broken down regionally using the United Nations sub-regions (UNSD, 1999) over SSA.

Climate mode	Percentage of river network with significant changes in impactful flood probability p_f at a 95%-confidence level (conditional on each climate mode)						
	Significant decrease, $p_f<15\%$	Significant increase, $p_f>25\%$					
	Whole SSA (%)	Whole SSA (%)	Eastern SSA (%)	Central SSA (%)	Western SSA (%)	Southern SSA (%)	Northern SSA (%)
ENSO +	13	3	5	2	3	< 1	1
ENSO –	10	10	8	12	4	25	14
IOD +	12	4	6	5	3	< 1	1
IOD –	14	6	5	7	12	< 1	< 1
TSA +	12	10	6	9	9	18	17
TSA –	19	7	9	8	8	1	3

(iv) For IOD – (Fig. 2d): flood likelihood increases in western SSA including long river sections of the Niger basin, in parts of central SSA, including some minor northern sections of the Congo basin and neighbouring basins above the equator; it decreases in central SSA, including long river sections in the upstream Congo basin across DRC, in the upper Zambezi basin (mainly in Zambia and Malawi) and in northern Mozambique, including the Rovuma and Lugenda Rivers.

(v) For TSA + (Fig. 2e): flood likelihood increases mainly in southern Africa (below 10° S) including long sections of the Zambezi and

Okavango basin, in tropical northern SSA, mainly in long sections of the Bahr al-Arab River in the Nile Basin and in the Chari River along the Sahel, and in some river sections in the northern arc of the Gulf of Guinea region; it decreases mainly in central-equatorial SSA, particularly in central/northern parts of the Congo basin (across the DRC and Republic of the Congo).

(vi) For TSA – (Fig. 2f): flood likelihood increases in central-western SSA, particularly the southern arc of the Gulf of Guinea region and upstream sections of the Congo basin (in the Republic of the

Table 3
Contingency tables summarizing the agreement in changes in flood likelihood of the impactful flood (5-year return period) between the GloFAS reanalysis and stream gauge observations during ENSO, IOD and TSA positive and negative phases at forty-eight stream gauges across SSA with observed daily data available over 1980–2015 (>27 years).

	ENSO + years	**Observations**			
		Significant increase > 25%	Increase (non sig.)	Decrease (non sig.)	Significant decrease < 15%
GloFAS	Significant increase > 25%	0	0	2	0
	Increase (non sig.)	2	3	14	1
	Decrease (non sig.)	2	4	9	1
	Significant decrease < 15%	0	1	4	1
	ENSO - years	**Observations**			
		Significant increase > 25%	Increase (non sig.)	Decrease (non sig.)	Significant decrease < 15%
GloFAS	Significant increase > 25%	6	4	0	0
	Increase (non sig.)	1	14	0	1
	Decrease (non sig.)	1	7	1	0
	Significant decrease < 15%	2	6	2	0
	IOD + years	**Observations**			
		Significant increase > 25%	Increase (non sig.)	Decrease (non sig.)	Significant decrease < 15%
GloFAS	Significant increase > 25%	1	1	0	0
	Increase (non sig.)	0	9	4	0
	Decrease (non sig.)	0	6	15	2
	Significant decrease < 15%	0	4	1	0
	IOD - years	**Observations**			
		Significant increase > 25%	Increase (non sig.)	Decrease (non sig.)	Significant decrease < 15%
GloFAS	Significant increase > 25%	0	0	3	0
	Increase (non sig.)	0	5	7	5
	Decrease (non sig.)	1	3	13	3
	Significant decrease < 15%	0	1	3	1
	TSA + years	**Observations**			
		Significant increase > 25%	Increase (non sig.)	Decrease (non sig.)	Significant decrease < 15%
GloFAS	Significant increase > 25%	3	2	0	0
	Increase (non sig.)	5	16	1	1
	Decrease (non sig.)	4	5	1	2
	Significant decrease < 15%	4	0	1	0
	TSA- years	**Observations**			
		Significant increase > 25%	Increase (non sig.)	Decrease (non sig.)	Significant decrease < 15%
GloFAS	Significant increase > 25%	0	3	2	0
	Increase (non sig.)	0	4	9	0
	Decrease (non sig.)	0	1	16	3
	Significant decrease < 15%	0	0	4	2

(Total) All modes– **matching observations and GloFAS reanalysis for each mode**		**Observations**			
		Significant increase > 25%	Increase (non sig.)	Decrease (non sig.)	Significant decrease < 15%
GloFAS	Significant increase > 25%	10	10	7	0
	Increase (non sig.)	8	51	35	8
	Decrease (non sig.)	8	26	55	11
	Significant decrease < 15%	6	12	15	4

Congo), in some parts of eastern Africa, especially the Jubba-Shabelle basin (in Ethiopia and Somalia); it decreases mainly in central-southern SSA (particularly between 5° S and 20° S) and in portions of tropical northern SSA, particularly in the Nile basin.

Apart from these broad patterns, there is a complex and noisy spatial signal of flood likelihood changes with some river sections presenting a different (sometimes opposite) signal of change within the same catchment, thus cancelling each other out downstream. These results of some broad patterns within a noisy picture are in line with previous studies on the effects of ENSO on streamflow at the global scale and confirm the importance of looking at how the hydrology alters the patterns seen in precipitation (Emerton et al., 2017). The significant signal detected from the streamflow reanalysis is confirmed by the observational dataset for three out of the six biggest river basins (Congo, Nile, and Zambezi) with the same significant impacts of climate variability on floods. The consistency between reanalysis and observations is lower for two other top-five river basins (Orange and Niger) and for a few smaller basins in southern Africa. A statistical evaluation of the consistency between reanalysis and observations based on our composite analysis (Table 3) shows a perfect agreement (same significant changes) in 45% of cases and at least partial agreement (same sign of change) in 62% of cases, which is limited by the higher density of stations in the Niger and Orange basins where the consistency is found lower (i.e. likely to be due to higher impacts of human influence on those stream gauges).

The percentage of river network presenting significant changes (either increase or decrease) in flood likelihood is similar across all the climate modes considered and ranges between 16 and 26% (Table 2) which is generally higher than significant changes expected from randomised samples (see Section 2, Data and Methods). For all climate modes, there are more points with significant signal of change in flood likelihood with negative phases than positive ones. The extent of the river network affected by significant increases in flood likelihood is highest for La Niña and TSA+ (10%). The extent of the river network affected by a significant decrease in flood likelihood is larger than for significant increase for all climate modes except for La Niña years for which it is equal (10%). Table 2 shows that the modes driving increase in flood hazard in larger contiguous areas (>10% of the river network) are: (i) ENSO - especially in southern SSA, (ii) IOD – in western SSA, and (iii) TSA + in southern and northern SSA. The results should be interpreted more cautiously where the GEV fit is poorer, i.e. areas with large absolute values of the shape parameter, mainly in southern and eastern Africa (see Supplementary Fig. S4).

The numbers in the tables represent the counts of river cells with p_f changes matching the categories in the column (observations) and row (reanalysis) headers. The last contingency table (Total) sums up all composite modes (with all pairs of observations/reanalysis derived summing up all stream gauges for the six different climate modes and removing a few combinations of river cells/climate modes with unsatisfactory GEV fit). Statistical tests outputs from the total contingency table: McNemar's Chi-squared test ($p = 0.17$, H0: the two marginal probabilities are the same) and Dependent-samples Sign-Test ($p = 0.80$, H0: median difference is equal to 0). The percent correct (i.e. diagonal, or agreement with significance) is 45%, while the agreement without significance is 62% (i.e. percent correct from reduced 2 × 2 table).

Fig. 3 shows a comparative analysis of the impact of ENSO/IOD/TSA phases on flood hazard increase across SSA from the reanalysis and available stream gauge data. Despite the general noise found in the distribution of the areas-of-influence of each climate mode (Fig. 2), multiple and long river sections up to several hundreds of km across SSA can be associated to a dominant climate mode driving increased flood hazard (Fig. 3). For example, in each of the six major African river basins, the most influential climate modes to drive increased flood hazard can be found by detecting the mode with the highest increase in flood likelihood in the downstream river sections or with the most widespread influence over the basin from the reanalysis (Figs. 3 and 4). The Congo

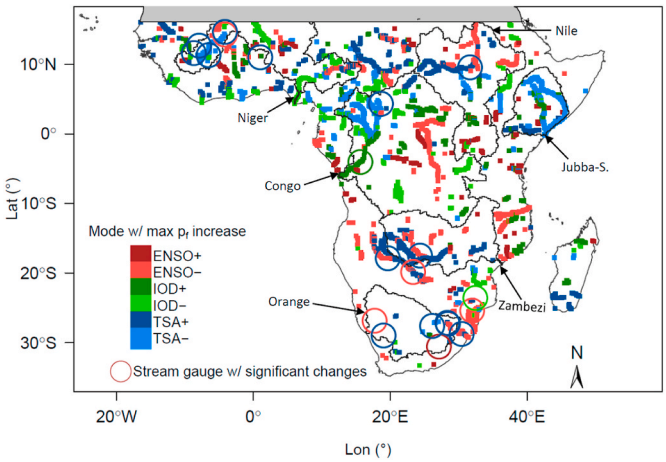

Fig. 3. Map of SSA highlighting the dominant climate mode (among positive and negative ENSO, IOD, TSA phases) for significant increase in flood hazard (p_f>25% at a 95%-confidence level) for all river cells from the streamflow reanalysis and 21 stream gauges (out of 48 with sufficiently long records) where significant increases in 5-year return level flood probability are found (circle dots). The boundaries of the six major SSA river basins are drawn (black line) with labels indicating the river basin name.

basin is more affected by IOD+ in its downstream sections than any other mode but presents longer river sections upstream which are more impacted by TSA- and by La Niña; the dominance of IOD + as driver of increased flood hazard in the lower Congo is confirmed by stream-gauge data (Fig. 3). The sub-Saharan portion of the Nile basin (up to Wad Ramli, near Khartoum in Sudan) is mostly affected by La Niña and TSA+, as also confirmed by stream-gauge data (Figs. 2 and 3). The Niger basin (including the Benue River, Niger's main tributary) is mostly affected by IOD- and TSA-based on the reanalysis, but this is not confirmed by stream-gauge data which show a dominant impact of TSA+ (Fig. 3). In the Zambezi basin, long upstream sections of around 1000 km are mostly affected by TSA+ (Fig. 3), especially along the Cuando-Linyanti-Chobe river system, where also La Niña has a widespread impact; this dominance of TSA+ is confirmed by stream-gauge data (Fig. 3). The Jubba-Shabelle river basin in Ethiopia and Somalia is mostly affected by TSA-with the whole main river system significantly affected, while long sections are also affected by IOD+, which is the second mode in the basin in terms of most widespread impacts (Figs. 3 and 4), despite being more prominent than TSA in the literature on local rainfall teleconnections (see Section 4, Discussion and Conclusions); however, the two stream gauges available in this basin do not show any significant change. Among the six biggest African river catchments, the Orange river presents the least widespread impacts, with La Niña and TSA + having the biggest influence but only in relatively short river sections (Fig. 3); this is in partial agreement with results from stream-gauge data showing a prevalent impact of TSA+. Among other minor but long rivers associated to a dominant climate mode for increased flood hazard one of the most evident (Fig. 3) is the Rovuma River (in northern Mozambique) which is more affected by La Niña than any other mode.

Overall, where flood likelihood increases significantly, the new increased 5-year flood probabilities show similar distributions across different climate modes over SSA (Fig. 4a) even if the extent of the river network affected by each mode is different. For all river cells with significant increase in flood likelihood, the median probability of the impactful flood is around 40% for all positive/negative phases considered (Fig. 4a) and the highest probabilities (e.g. 90th-percentile) are between 50 and 60%. More differences in the probability distribution emerge when results are aggregated at the catchment level (Fig. 4b).

A first assessment of the impact of co-occurrent climate modes indicates that the interaction between modes may lead to marked changes

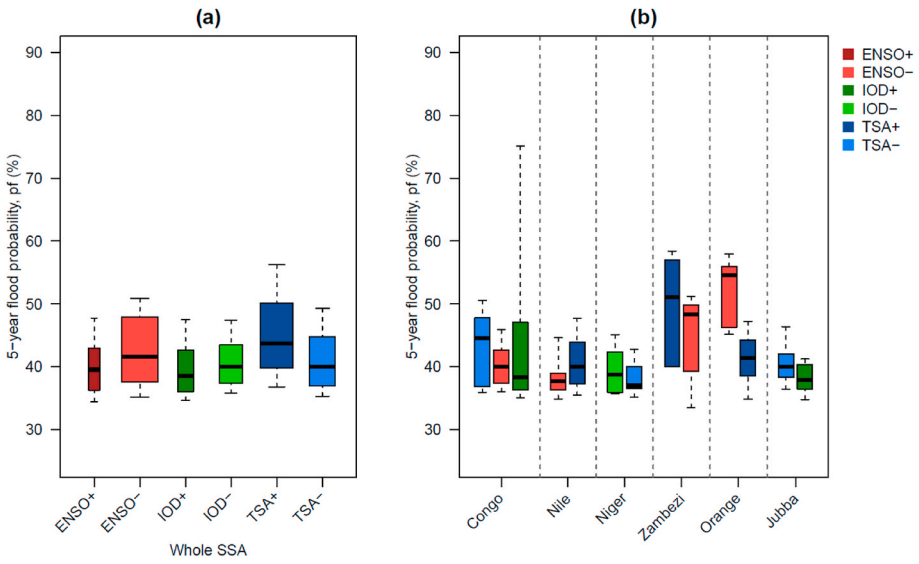

Fig. 4. Boxplot with distribution of the 5-year flood probabilities for all climate modes over whole SSA (a), and for the most influential modes over the six major river basins (b) from the streamflow reanalysis. The most influential modes are defined as the ones with the biggest significant impact in downstream sections (i.e. top 95% upstream areas), when significant changes are present, and the top two modes with the most widespread influence over the basin (with significant increase for at least 5% of the river network). The boxplots report the median value, interquartile range, and the whiskers represent the 10th and 90th percentiles; the boxplots width in (a) is proportional to the number of river cells significantly affected for each climate mode, i.e. a box of given width for each mode in panel (a) represents the same number of cells.

in flood frequencies. In other words, the effects of a single mode can be different if only pure occurrences of a single mode or co-occurrences with another mode are considered, as found at some stream-gauges where long observed records are available (see Table S2). For instance, in the lower Congo basin our results suggest that pure occurrences of IOD+ (without concomitant ENSO+) may have a greater influence than co-occurrences of IOD+ and ENSO + to drive increased flood hazard, as seen from the river-gauge data available (Table S2) and from the differences in signal from the reanalysis despite the high co-occurrence rate between ENSO+ and IOD+ (Figs. 2–3).

Finally, we tested the sensitivity of the results with the return period varying from 2- to 10-year, finding that in general the same sign of changes (increase/decrease) of flood likelihood is expected for higher return periods but with higher uncertainty (see Supplementary Fig. S5; Tables S3–S4). While the agreement in the sign of changes of 5-yr and 10-yr return period flood likelihood is high, and similar spatial patterns can be found (Fig. S5 and Fig. 2), the river cells with significant increase in 5-year flood likelihood mostly show consistent increases of the 10-year flood likelihood but with low or no significance because of the limited sample of composite years (see Table S4).

3.2. Towards a forecasting application: Assessing the reliability of the flood probabilities

The historical probabilities for increased flood hazard can be assessed as probabilistic forecasts. Fig. 5 shows a reliability assessment for forecasts of increased impactful flood hazard (p_f>20%) for the positive and negative ENSO, IOD and TSA phases. For higher forecast probabilities, e.g. >80%, which are the most important for decisions, Fig. 5 suggests that: (i) on average, the negative phases seem more reliable than the correspondent positive phases for all climate modes; (ii) there is a large variability across different validation years for all climate modes, but for ENSO -, IOD + and TSA -, these flood forecasts are more reliable than climatology at 90%-confidence level; (iii) negative TSA phases seem to provide the most reliable predictions, while for the highest probabilities ENSO + and TSA + are the least reliable.

4. Discussion and conclusions

In summary, we find that the Indian Ocean Dipole and the Tropical South Atlantic SST modes are as influential as ENSO for driving flood hazard in Africa, with similar proportions of the continental river network affected by each and similar increased flood probabilities, but important spatial differences between the regions affected. This result urges a paradigm shift to give higher weight to other modes of climate variability when considering the drivers of floods across Africa, both for improvements to early warning systems and to our understanding of the impacts of future climate change. Because these climate modes operate concurrently in some cases, further research is needed on the interaction effects on flood hazard when different modes are in or out of phase at the same time. A limitation of our study is that the 36-year data available do not allow to separate the effects of co-occurrent modes, which would require a larger sample of years for streamflow data. Another limitation linked to the small sample size of data available is that we cannot extrapolate our findings for higher return periods (than 5-year) with sufficient statistical confidence. This highlights the need for longer observed streamflow records over Africa, with less sparse coverage than what available so far (at least in publicly available archives). In their absence, more efforts should be made to produce longer hydrological reanalyses incorporating observed meteorological data for bias correction.

What are our main findings on the effects of ENSO on flood hazard and how do they compare with the literature? For ENSO, the broad spatial patterns in the change in flood hazard and the dominance of La Niña rather than El Niño in increasing flood hazard over Africa are consistent with previous studies (Emerton et al., 2017; Ward et al., 2014a, 2014b). The widespread influence of La Niña (El Niño) in driving (reducing) floods in the Nile Basin is in agreement with previous studies (Amarasekera et al., 1997; Eltahir, 1996). These consistent comparisons give us confidence in our assessment of the relative importance of other modes of climate variability. In eastern Africa, despite the known wet anomalies in rainfall in the region in El Niño years (and IOD + years), only a few smaller basins were found with higher annual floods. This can be explained by the fact that the rainfall anomalies with ENSO + (and IOD+) are found in the short-rains season from October to following January (Guimarães Nobre et al., 2019) which does not correspond to the average annual flood timing in the region which is mainly in April–June following the long rains (Ficchì and Stephens, 2019). An exception to this pattern in eastern Africa is the Jubba-Shabelle basin where for the main rivers flood timing falls in the short-rains season (Ficchì and Stephens, 2019), as it is influenced by larger runoff contributions from upstream areas in the Ethiopian highlands, where rainfall teleconnections with IOD + are more prominent than ENSO (Behera et al., 2005; Black, 2005); this explains why the IOD + has the second most widespread impact in this basin. On the other hand, with La Niña the wetter than normal period in southern Africa is November to

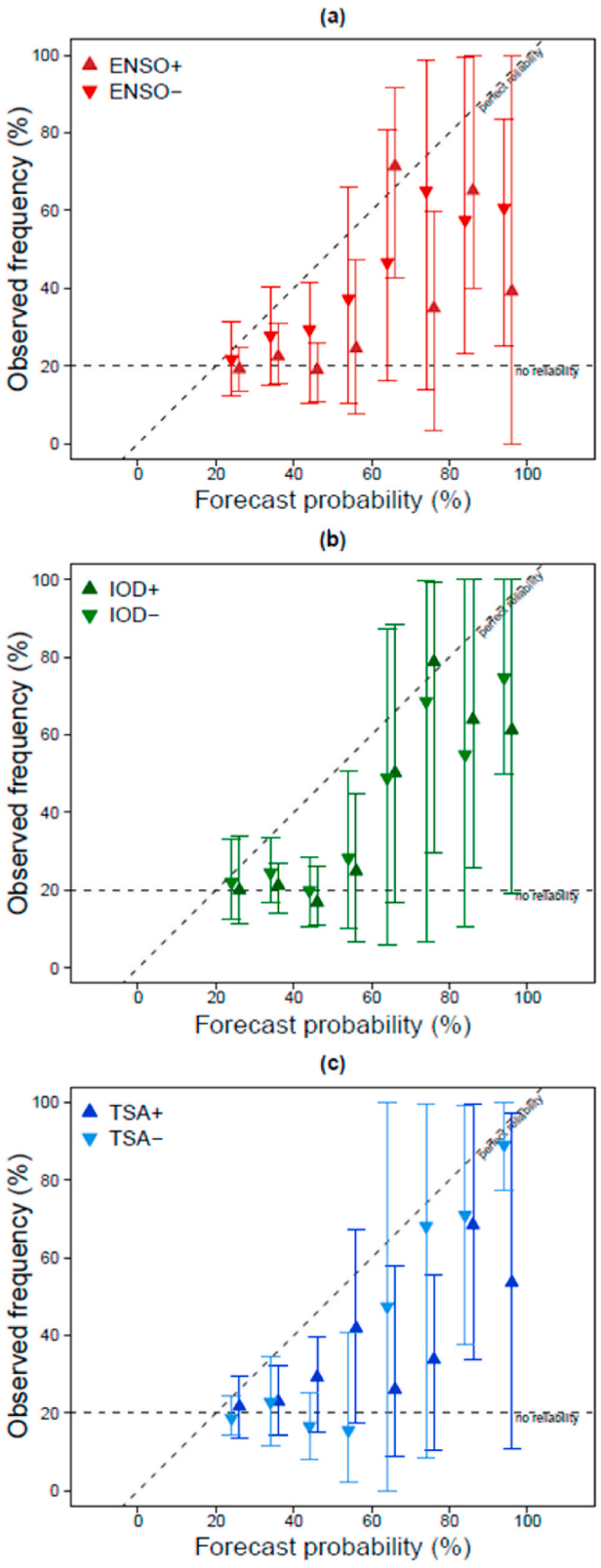

Fig. 5. Reliability diagram of the increase in mean exceedance probability for the impactful flood (climatology 5-year return level) for positive and negative (a) ENSO, (b) IOD and (c) TSA phases vs. observed frequency; the triangular dots show the average of the observed frequency for all the validation years, with error bar at 90%-confidence interval based on the validation years bootstrap set.

following April and in northern tropical SSA is July to September which do correspond to the local annual flood seasons; this synchronicity between the timing of the rainfall anomalies and annual floods contributes to a stronger signal of increased flood hazard with La Niña.

What is the relative weight of different climate modes on floods at the continental scale? The ENSO, IOD and TSA modes showed similar weight in terms of the spatial extent of the continental river network affected by changes in flood likelihood, with a portion of rivers affected by significant changes (increase or decrease) ranging between 16% and 26% across sub-Saharan Africa. On average, the increased flood probabilities are also similar for all modes across SSA and correspond to a doubling of the impactful flood probability for the rivers affected by significant increase.

Where is each climate mode dominant? We find a high spatial dispersion of the significant changes in floods for the different modes of climate variability, with contrasting behaviour across some regions and low signal-to-noise ratios, consistently with previous studies on hydrological interannual variability across SSA (Conway et al., 2009; Sidibe et al., 2019). Despite this, we also identify some strong signals from dominant modes that emerge for long river sections in some of the major African basins from the reanalysis and are validated by observations available for the Congo, Nile, and Zambezi river basins.

In central Africa, the IOD and TSA modes showed larger effects on flood hazard than ENSO, especially in the Congo River Basin where IOD + has the greatest influence downstream and in the neighbour areas in southern central Africa where the leading impacts come from TSA+. This result is consistent with the previous literature on teleconnections, showing a weak link between El Niño and regional rainfall and total annual Congo River discharge (Amarasekera et al., 1997; Camberlin et al., 2001; Todd and Washington, 2004) and a major link between wet rainfall anomalies and SSTs in the central tropical Indian Ocean (Nicholson and Dezfuli, 2013) and tropical southern Atlantic (Camberlin et al., 2001; Hirst and Hastenrath, 1983; Nicholson and Entekhabi, 1987). Research by Becker et al. (2018) indicates that large positive anomalies of lakes and river levels in the Congo River Basin (obtained from remote sensing and in situ data) over the period 1993–2007 followed two positive IOD events occurring in conjunction with an El Niño event (1997–1998 and 2006–2007). Our results over a longer period agree with the importance of IOD+ and suggest its independence and dominant role over ENSO+ in driving floods in the basin (see Fig. 3, and Supplementary Table S2). Warm water anomalies in the South Atlantic (TSA+) showed the largest effects on increased flood hazard across large parts of southern Africa especially in the Zambezi and Okavango basins. This result is particularly important as previous studies tend to regard the western Indian Ocean as the primary source of moisture for austral summer rainfall over southern Africa and the south Atlantic as a secondary source (Rouault et al., 2003). However, the literature on rainfall teleconnections shows signals of above average rainfall in coastal but also inland areas of southern Africa with warm tropical South Atlantic SSTs (Manhique et al., 2015; Williams et al., 2008) which can explain our results on the role of TSA to drive annual floods in the region. In southern Africa, also La Niña has a dominant impact on increased flood hazard, consistently with earlier findings on its influence on rainfall (Nicholson and Selato, 2000); this result can be linked also to the high rate of co-occurrence between La Niña and warm TSA events (see Supplementary Fig. S2 and Table S1).

Our new finding of the dominant links of TSA with the Jubba-Shabelle river system in eastern Africa is important and surprising because there is little known about analogous rainfall teleconnections in the region and the basin is far beyond the regions bordering the Atlantic Ocean. We suggest that the increased flood hazard is explained by the fact that the basin receives the largest runoff contributions from the northern summer rains over Ethiopia which are known to be related to the monsoon air flow from the Congo Basin and the Atlantic Ocean (Beltrando and Camberlin, 1993; Camberlin et al., 2001; Rowell, 2013) and Ethiopian monsoon rainfall is enhanced in association with cold SST

anomalies over the South Atlantic Ocean (Segele et al., 2009) with augmented westerly wind and moisture flux into Ethiopia.

Can these climate modes be used for flood forecasting? Historical flood probabilities based on ENSO have been shown to outperform dynamical modelling approaches in many parts of Africa (Emerton et al., 2019). Our first assessment of the reliability of probabilistic flood forecasts for different climate modes suggests that the Indian Ocean and Atlantic modes may provide more reliable flood forecasts than the Pacific El Niño overall across Africa. We have verified the forecasts across all the gridcells in sub-Saharan Africa, with a large spatial aggregation level which was necessary given the limited sample of years at each location. Further research should look at the reliability of these forecasts for smaller geographical regions as more data would become available, to map regions with more reliable forecasts. As our analysis is based on observed climate indices, the potential for using predicted SST indices for flood forecasts and early warning should be further explored considering the skill of the climate indices forecasts at relevant lead time for decision making. At a very minimum, these statistical forecasts should be used as a benchmark for dynamical seasonal hydrological forecasts for Africa.

What are the implications of our results for the assessment of flood hazard under climate change? Within the IPCC process ENSO dominates the conversation when considering climate extremes (e.g. SREX report), but our results on the impact of different modes of climate variability on flood hazard highlight that other modes in the Indian Ocean and Atlantic should be higher up the agenda when it comes to climate model evaluation, development and process-based analysis of simulated extremes (Sillmann et al., 2017). For example, our results suggest that the IOD plays a similar role to ENSO, which highlights the importance of understanding how the IOD might change in the future. The frequency of occurrences of positive IOD events in recent decades has increased (Abram et al., 2008) and is expected to continue increasing in the future with increased greenhouse gases (Cai and Cowan, 2013) even if large uncertainties remain in the projected future changes (Endris et al., 2019). However climate models are known to overrepresent the amplitude of the IOD (Cai and Cowan, 2013) which leads to bias in the East-African short rains (Hirons and Turner, 2018). For the Tropical Atlantic SSTs, there is still much scope for improving the skill of forecasts of SST anomalies (Stockdale et al., 2006) which are known to be crucial to simulate atmospheric circulation and precipitation over Africa (Eichhorn and Bader, 2017). Our results confirm the importance of this, given the significant role of Tropical South Atlantic for driving flood hazard across Africa.

Data availability

The GloFAS-ERA-Interim/Land streamflow reanalysis data that support the findings of this study are available from the corresponding author upon request or may be provided through an ftp service setup by the GloFAS team, by contacting the operational service at info@globalfloods.eu (see www.globalfloods.eu). The Global Runoff Data Centre (GRDC) provided the observed streamflow data set which is publicly available (www.bafg.de/GRDC). The climate indices that support the findings of this study are publicly available online, as reported in Section 2, Data and Methods.

Code availability

All the analysis presented in this paper was performed in R (R Core Team, 2017). The GEV fit functions and the parametric bootstrapping algorithm are available in the R package 'extRemes' (Gilleland and Katz, 2016). The R scripts used to generate the results described in the paper are available from the corresponding author upon request.

Author contributions

A.F. carried out the analysis and wrote the first draft of the paper. A. F., E.S., H.C., C.N. and S.W. conceived the research questions, designed the study and interpreted the results. E.Z. produced the GloFAS-ERA-Interim/Land streamflow reanalysis data set and interpreted the results. All authors discussed the results and their implications and commented and contributed to the manuscript.

Andrea Ficchì: Conceptualization, Data curation, Methodology, Investigation, Software, Formal analysis, Visualization, Project administration, Writing – original draft, Writing - Review & Editing. **Hannah Cloke**: Conceptualization, Methodology, Investigation, Writing – original draft, Writing - Review & Editing, Project administration, Supervision. **Claudia Neves**: Methodology, Formal analysis, Investigation, Writing – original draft. **Steve Woolnough**: Conceptualization, Methodology, Writing – original draft. **Erin Coughlan de Perez**: Conceptualization, Methodology, Writing – original draft. **Ervin Zsoter**: Data curation, Methodology, Investigation, Writing – original draft. **Izidine Pinto**: Investigation, Writing – original draft. **Arlindo Meque**: Investigation, Writing – original draft. **Elisabeth Stephens**: Conceptualization, Methodology, Investigation, Writing – original draft, Writing - Review & Editing, Project administration, Supervision, Funding acquisition.

Declaration of competing interest

The authors declare that they have no known competing financial interests or personal relationships that could have appeared to influence the work reported in this paper.

Acknowledgments

The authors acknowledge the support by the Natural Environment Research Council (NERC) and Foreign, Commonwealth and Development Office (FCDO), formerly Department for International Development (grant number NE/P000525/1), under the Science for Humanitarian Emergencies and Resilience (SHEAR) research programme. Steve Woolnough's contribution was also supported by National Centre for Atmospheric Science ODA national capability programme ACREW (NE/R000034/1), which is supported by NERC and the GCRF. Claudia Neves gratefully acknowledges support from EPSRC-UKRI Innovation Fellowship grant EP/S001263/1. We thank colleagues from the FATHUM and ForPAc projects, and associated project partners (ECMWF and JRC) for the useful discussions related to this work. We would like to acknowledge the anonymous reviewer and the Editor-in-Chief, Lisa Alexander, for their valuable comments and suggestions.

Appendix A. Supplementary data

Supplementary data to this article can be found online at https://doi.org/10.1016/j.wace.2021.100345.

References

Abram, N.J., Gagan, M.K., Cole, J.E., Hantoro, W.S., Mudelsee, M., 2008. Recent intensification of tropical climate variability in the Indian Ocean. Nat. Geosci. 1 (12), 849–853. https://doi.org/10.1038/ngeo357.

Alfieri, L., et al., 2013. GloFAS – global ensemble streamflow forecasting and flood early warning. Hydrol. Earth Syst. Sci. 17 (3), 1161–1175. https://doi.org/10.5194/hess-17-1161-2013.

Amarasekera, K.N., Lee, R.F., Williams, E.R., Eltahir, E.A.B., 1997. ENSO and the natural variability in the flow of tropical rivers. J. Hydrol. 200 (1–4), 24–39. https://doi.org/10.1016/s0022-1694(96)03340-9.

Balsamo, G., et al., 2015. ERA-Interim/Land: a global land surface reanalysis data set. Hydrol. Earth Syst. Sci. 19 (1), 389–407. https://doi.org/10.5194/hess-19-389-2015.

Becker, M., et al., 2018. Satellite-based estimates of surface water dynamics in the Congo River Basin. Int. J. Appl. Earth Obs. Geoinf. 66, 196–209. https://doi.org/10.1016/j.jag.2017.11.015.

Behera, S.K., et al., 2005. Paramount impact of the Indian Ocean Dipole on the East african short rains: a CGCM study. J. Clim. 18 (21), 4514–4530. https://doi.org/10.1175/jcli3541.1.
Beltrando, G., Camberlin, P., 1993. Interannual variability of rainfall in the eastern horn of Africa and indicators of atmospheric circulation. Int. J. Climatol. 13 (5), 533–546. https://doi.org/10.1002/joc.3370130505.
BfG, 2017. The global runoff data base (GRDB). In: GRDC. Retrieved from:. http://grdc.bafg.de/.
Black, E., 2005. The relationship between Indian Ocean sea–surface temperature and East African rainfall. Phil. Trans. Math. Phys. Eng. Sci. 363 (1826), 43–47. https://doi.org/10.1098/rsta.2004.1474.
Cai, W., Cowan, T., 2013. Why is the amplitude of the Indian Ocean Dipole overly large in CMIP3 and CMIP5 climate models? Geophys. Res. Lett. 40 (6), 1200–1205. https://doi.org/10.1002/grl.50208.
Cai, W., Rensch, P.v., Cowan, T., Hendon, H.H., 2011. Teleconnection pathways of ENSO and the IOD and the mechanisms for impacts on Australian rainfall. J. Clim. 24 (15), 3910–3923. https://doi.org/10.1175/2011jcli4129.1.
Cai, W., et al., 2015. ENSO and greenhouse warming. Nat. Clim. Change 5 (9), 849–859. https://doi.org/10.1038/nclimate2743.
Camberlin, P., Janicot, S., Poccard, I., 2001. Seasonality and atmospheric dynamics of the teleconnection between African rainfall and tropical sea-surface temperature: Atlantic vs. ENSO. Int. J. Climatol. 21 (8), 973–1005. https://doi.org/10.1002/joc.673.
Conway, D., et al., 2009. Rainfall and water resources variability in sub-saharan Africa during the twentieth century. J. Hydrometeorol. 10 (1), 41–59. https://doi.org/10.1175/2008jhm1004.1.
Coughlan de Perez, E., et al., 2015. Forecast-based financing: an approach for catalyzing humanitarian action based on extreme weather and climate forecasts. Nat. Hazards Earth Syst. Sci. 15 (4), 895–904. https://doi.org/10.5194/nhess-15-895-2015.
ECMWF, 2018. GloFAS v1.0. In: CEMS-floods. Copernicus Emergency Management Service - CEMS.. http://confluence.ecmwf.int/display/COPSRV/GloFAS+v1.0.
Eichhorn, A., Bader, J., 2017. Impact of tropical Atlantic sea-surface temperature biases on the simulated atmospheric circulation and precipitation over the Atlantic region: an ECHAM6 model study. Clim. Dynam. 49 (5), 2061–2075. https://doi.org/10.1007/s00382-016-3415-x.
Eltahir, E.A.B., 1996. El Niño and the natural variability in the flow of the nile river. Water Resour. Res. 32 (1), 131–137. https://doi.org/10.1029/95wr02968.
Emerton, R., et al., 2017. Complex picture for likelihood of ENSO-driven flood hazard. Nat. Commun. 8, 14796. https://doi.org/10.1038/ncomms14796.
Emerton, R., Stephens, E., Cloke, H., 2019. What is the most useful approach for forecasting hydrological extremes during El Niño? Environ. Res. Commun. 1, 31002.
Endris, H.S., et al., 2019. Future changes in rainfall associated with ENSO, IOD and changes in the mean state over Eastern Africa. Clim. Dynam. 52 (3), 2029–2053. https://doi.org/10.1007/s00382-018-4239-7.
Enfield, D.B., Mestas-Nuñez, A.M., Mayer, D.A., Cid-Serrano, L., 1999. How ubiquitous is the dipole relationship in tropical Atlantic sea surface temperatures? J. Geophys. Res.: Oceans 104 (C4), 7841–7848. https://doi.org/10.1029/1998JC900109.
Ficchì, A., Stephens, L., 2019. Climate variability alters flood timing across Africa. Geophys. Res. Lett. 46 (15), 8809–8819. https://doi.org/10.1029/2019gl081988.
Florenchie, P., Lutjeharms, J.R.E., Reason, C.J.C., Masson, S., Rouault, M., 2003. The source of Benguela niños in the south Atlantic Ocean. Geophys. Res. Lett. 30 (10) https://doi.org/10.1029/2003GL017172.
Gilleland, E., Katz, R., 2016. extRemes 2.0: an extreme value analysis package in R. J. Stat. Software 72 (8), 1–39. https://doi.org/10.18637/jss.v072.i08.
Guimarães Nobre, G., Muis, S., Veldkamp, T.I.E., Ward, P.J., 2019. Achieving the reduction of disaster risk by better predicting impacts of El Niño and La Niña. Progr. Disast. Sci. 2, 100022. https://doi.org/10.1016/j.pdisas.2019.100022.
Hirons, L., Turner, A., 2018. The impact of Indian ocean mean-state biases in climate models on the representation of the East african short rains. J. Clim. 31 (16), 6611–6631. https://doi.org/10.1175/jcli-d-17-0804.1.
Hirst, A.C., Hastenrath, S., 1983. Diagnostics of hydrometeorological anomalies in the Zaire (Congo) basin. Q. J. R. Meteorol. Soc. 109 (462), 881–892. https://doi.org/10.1002/qj.49710946213.
Horritt, M.S., 2006. A methodology for the validation of uncertain flood inundation models. J. Hydrol. 326 (1), 153–165. https://doi.org/10.1016/j.jhydrol.2005.10.027.
IASC, 2018. Inter-Agency SOPs for Early Action to El Niño/La Niña Episodes. Inter-Agency Standing Committee.
Jury, M.R., Lucio, F.D.E., 2004. The Mozambique floods of February 2000 in context. S. Afr. Geogr. J. 86 (2), 141–146. https://doi.org/10.1080/03736245.2004.9713818.
Lutz, K., Jacobeit, J., Rathmann, J., 2015. Atlantic warm and cold water events and impact on African west coast precipitation. Int. J. Climatol. 35 (1), 128–141. https://doi.org/10.1002/joc.3969.
Lutz, K., Rathmann, J., Jacobeit, J., 2013. Classification of warm and cold water events in the eastern tropical Atlantic Ocean. Atmos. Sci. Lett. 14 (2), 102–106. https://doi.org/10.1002/asl2.424.
Lyon, B., Mason, S.J., 2007. The 1997–98 summer rainfall season in southern Africa. Part I: observations. J. Clim. 20 (20), 5134–5148. https://doi.org/10.1175/jcli4225.1.
Manatsa, D., Chingombe, W., Matarira, C.H., 2008. The impact of the positive Indian Ocean dipole on Zimbabwe droughts. Int. J. Climatol. 28 (15), 2011–2029. https://doi.org/10.1002/joc.1695.
Manhique, A.J., et al., 2015. Extreme rainfall and floods in southern Africa in January 2013 and associated circulation patterns. Nat. Hazards 77 (2), 679–691. https://doi.org/10.1007/s11069-015-1616-y.
Marchant, R., Mumbi, C., Behera, S., Yamagata, T., 2007. The Indian Ocean dipole – the unsung driver of climatic variability in East Africa. Afr. J. Ecol. 45 (1), 4–16. https://doi.org/10.1111/j.1365-2028.2006.00707.x.
Nicholson, S.E., 2017. Climate and climatic variability of rainfall over eastern Africa. Rev. Geophys. 55 (3), 590–635. https://doi.org/10.1002/2016RG000544.
Nicholson, S.E., Dezfuli, A.K., 2013. The relationship of rainfall variability in western equatorial Africa to the tropical oceans and atmospheric circulation. Part I: the boreal spring. J. Clim. 26 (1), 45–65. https://doi.org/10.1175/jcli-d-11-00653.1.
Nicholson, S.E., Entekhabi, D., 1987. Rainfall variability in equatorial and southern Africa: relationships with sea surface temperatures along the southwestern coast of Africa. J. Clim. Appl. Meteorol. 26 (5), 561–578. https://doi.org/10.1175/1520-0450(1987)026<0561:rvieas>2.0.co;2.
Nicholson, S.E., Kim, J., 1997. The relationship of the El Niño–Southern Oscillation to African rainfall. Int. J. Climatol. 17 (2), 117–135. https://doi.org/10.1002/(SICI)1097-0088(199702)17:2<117::AID-JOC84>3.0.CO;2-O.
Nicholson, S.E., Selato, J.C., 2000. The influence of La Nina on African rainfall. Int. J. Climatol. 20 (14), 1761–1776.
Polo, I., Rodríguez-Fonseca, B., Losada, T., García-Serrano, J., 2008. Tropical atlantic variability modes (1979–2002). Part I: time-evolving SST modes related to West African rainfall. J. Clim. 21 (24), 6457–6475. https://doi.org/10.1175/2008jcli2607.1.
Preethi, B., Sabin, T.P., Adedoyin, J.A., Ashok, K., 2015. Impacts of the ENSO modoki and other tropical indo-pacific climate-drivers on african rainfall. Sci. Rep. 5, 16653. https://doi.org/10.1038/srep16653.
Reason, C.J.C., Rouault, M., 2002. ENSO-like decadal variability and South African rainfall. Geophys. Res. Lett. 29 (13) https://doi.org/10.1029/2002GL014663, 16-1-16-4.
Reason, C.J.C., Rouault, M., 2006. Sea surface temperature variability in the tropical southeast Atlantic Ocean and West African rainfall. Geophys. Res. Lett. 33 (21) https://doi.org/10.1029/2006GL027145.
Rouault, M., Florenchie, P., Fauchereau, N., Reason, C.J.C., 2003. South East tropical Atlantic warm events and southern African rainfall. Geophys. Res. Lett. 30 (5) https://doi.org/10.1029/2002GL014840.
Rowell, D.P., 2013. Simulating SST teleconnections to Africa: what is the state of the art? J. Clim. 26 (15), 5397–5418. https://doi.org/10.1175/jcli-d-12-00761.1.
Saji, N.H., Goswami, B.N., Vinayachandran, P.N., Yamagata, T., 1999. A dipole mode in the tropical Indian Ocean. Nature 401 (6751), 360–363.
Saji, N.H., Yamagata, T., 2003. Possible impacts of Indian Ocean Dipole mode events on global climate. Clim. Res. 25 (2), 151–169. https://doi.org/10.3354/cr025151.
Segele, Z.T., Lamb, P.J., Leslie, L.M., 2009. Seasonal-to-Interannual variability of Ethiopia/horn of Africa monsoon. Part I: associations of wavelet-filtered large-scale Atmospheric circulation and global sea surface temperature. J. Clim. 22 (12), 3396–3421. https://doi.org/10.1175/2008JCLI2859.1.
Shi, L., et al., 2012. How predictable is the Indian Ocean Dipole? Mon. Weather Rev. 140 (12), 3867–3884. https://doi.org/10.1175/mwr-d-12-00001.1.
Sidibe, M., et al., 2019. Interannual to Multi-decadal streamflow variability in West and Central Africa: interactions with catchment properties and large-scale climate variability. Global Planet. Change 177, 141–156. https://doi.org/10.1016/j.gloplacha.2019.04.003.
Sillmann, J., et al., 2017. Understanding, modeling and predicting weather and climate extremes: challenges and opportunities. Weath. Clim. Extr. 18, 65–74. https://doi.org/10.1016/j.wace.2017.10.003.
Stockdale, T.N., Balmaseda, M.A., Vidard, A., 2006. Tropical atlantic SST prediction with coupled ocean–atmosphere GCMs. J. Clim. 19 (23), 6047–6061. https://doi.org/10.1175/JCLI3947.1.
Su, L., et al., 2018. Long-term trends in global river flow and the causal relationships between river flow and ocean signals. J. Hydrol. 563, 818–833. https://doi.org/10.1016/j.jhydrol.2018.06.058.
Todd, M.C., Washington, R., 2004. Climate variability in central equatorial Africa: influence from the Atlantic sector. Geophys. Res. Lett. 31 (23) https://doi.org/10.1029/2004GL020975.
Tozier de la Poterie, A.S., et al., 2018. Understanding the use of 2015–2016 El Niño forecasts in shaping early humanitarian action in Eastern and Southern Africa. Int. J. Disast. Risk Reduct. 30, 81–94. https://doi.org/10.1016/j.ijdrr.2018.02.025.
Trenberth, K.E., 1997. The definition of El Niño. Bull. Am. Meteorol. Soc. 78 (12), 2771–2778. https://doi.org/10.1175/1520-0477(1997)078<2771:tdoeno>2.0.co;2.
Trenberth, K.E., Caron, J.M., 2000. The southern oscillation revisited: sea level pressures, surface temperatures, and precipitation. J. Clim. 13 (24), 4358–4365. https://doi.org/10.1175/1520-0442(2000)013<4358:tsorsl>2.0.co;2.
UNSD, 1999. Standard Country or Area Codes for Statistical Use (M49), Series M, No. 49. UNSD. https://unstats.un.org/unsd/methodology/m49/.
Van Der Knijff, J.M., Younis, J., De Roo, A.P.J., 2010. LISFLOOD: a GIS-based distributed model for river basin scale water balance and flood simulation. Int. J. Geogr. Inf. Sci. 24 (2), 189–212. https://doi.org/10.1080/13658810802549154.
Ward, P.J., Eisner, S., Flörke, M., Dettinger, M.D., Kummu, M., 2014a. Annual flood sensitivities to El niño–southern oscillation at the global scale. Hydrol. Earth Syst. Sci. 18 (1), 47–66. https://doi.org/10.5194/hess-18-47-2014.
Ward, P.J., et al., 2014b. Strong influence of El Niño Southern Oscillation on flood risk around the world. Proc. Natl. Acad. Sci. Unit. States Am. 111 (44), 15659–15664. https://doi.org/10.1073/pnas.1409822111.
Washington, R., Preston, A., 2006. Extreme wet years over southern Africa: role of Indian Ocean sea surface temperatures. J. Geophys. Res. 111 (D15), D15104. https://doi.org/10.1029/2005JD006724.
Wenhaji Ndomeni, C., Cattani, E., Merino, A., Levizzani, V., 2018. An observational study of the variability of East African rainfall with respect to sea surface

temperature and soil moisture. Q. J. R. Meteorol. Soc. 144 (S1), 384–404. https://doi.org/10.1002/qj.3255.

Williams, C.J.R., Kniveton, D.R., Layberry, R., 2008. Influence of south atlantic sea surface temperatures on rainfall variability and extremes over southern Africa. J. Clim. 21 (24), 6498–6520. https://doi.org/10.1175/2008jcli2234.1.

Wolff, C., et al., 2011. Reduced interannual rainfall variability in east Africa during the last ice age. Science 333 (6043), 743–747. https://doi.org/10.1126/science.1203724.